Enhanced intensity-difference squeezing via energy-level modulations in hot atomic media

Da Zhang,[1] Changbiao Li,[1] Zhaoyang Zhang,[1] Yiqi Zhang,[1] Yanpeng Zhang,[1,*] and Min Xiao[2,3,†]

[1]*Key Laboratory for Physical Electronics and Devices of the Ministry of Education and Shaanxi Key Laboratory of Information Photonic Technique, Xi'an Jiaotong University, Xi'an 710049, China*

[2]*Department of Physics, University of Arkansas, Fayetteville, Arkansas 72701, USA*

[3]*National Laboratory of Solid State Microstructures and School of Physics, Nanjing University, Nanjing 210093, China*

(Received 27 November 2016; published 18 October 2017)

Narrow-band intensity-difference squeezing (IDS) beams have important applications in quantum metrology and gravitational wave detection. The best way to generate narrow-band IDS is to employ a parametrically amplified (PA) four-wave mixing (FWM) process in high-gain atomic media. Such IDS can be further enhanced by cascading multiple PA FWM processes in separate atomic media. The complicated experimental setup, added losses, and mechanical stability can limit the wide use of such a scheme in practical applications. Here we show that by modulating the internal energy level(s) with an additional laser (or lasers), the degree of original IDS can be substantially increased. With an initial IDS of (-3.6 ± 0.4) dB using a PA nondegenerate FWM process in a three-level Λ-type configuration, the degree of IDS can be enhanced to (-7.0 ± 0.4) dB or (-9.0 ± 0.4) dB when we use one (two) laser beam (beams) to modulate the involved ground (excited) state (states). Our results show a low-loss, robust, and efficient way to produce a high degree of IDS and facilitate its potential applications.

DOI: 10.1103/PhysRevA.96.043847

I. INTRODUCTION

Traditionally, quantum correlated bright laser beams are generated through parametrically amplified (PA) optical down-conversion processes in nonlinear optical crystals [1–4]. The produced entangled beams typically have broad spectral width and therefore short coherence time due to the broad phase-matching width in nonlinear crystals [5–7]. Recently, narrow-band bright entangled light beams have been produced through a PA four-wave mixing (FWM) process in high-gain atomic media [8]. The intensity-difference squeezing (IDS) between the two beams can reach -8.0 dB without compensating for any system noise or correcting for transmission or detection efficiency [9]. Subsequently, as much as -9.2 dB IDS has been reported by using a pair of high-quantum-efficiency photodiodes [10]. Several interesting applications of using such narrow-band entangled beams, such as in entangled images [11,12], FWM slow light [13], delay of Einstein-Podolsky-Rosen entanglement [14,15], and quantum metrology [16–21], have all been experimentally demonstrated. In order to further increase the degree of IDS, the technique of cascading more stages of the PA FWM process has been employed. In one experiment, a second PA FWM process in a separate atomic vapor cell was used to enhance the IDS from (-5.5 ± 0.1) dB or (-4.5 ± 0.1) dB to (-7.0 ± 0.1) dB [22]. Similarly, enhanced continuous-variable squeezed states have also been realized by cascading two PA down-conversion processes using two separate nonlinear crystals [23]. An ultimate enhancement limit reachable by using more stages of such cascade setups can be theoretically derived [24]. Although the cascading technique is conceptually simple to consider, the added complications in the experimental setup and the required high-power pump laser with the increase of number of stages, as well as maintaining the phase coherence, between different stages will severely limit the broad applications in using such a generated high degree of IDS.

Here we implement a totally different approach to enhance the IDS produced from the two correlated light beams generated from the PA FWM process in a three-level Λ-type atomic system. Since the degree of IDS is mainly determined by the high optical gain realizable in the PA FWM process [8], we set to find an efficient way to enhance the optical gain in the same atomic system: in our experiments, the dressing fields, to significantly improve the conversion efficiency in four-wave mixing as a major benefit of constructive interference between different transition probability amplitudes [25], which produces efficient higher-order multiwave mixing processes [26–28]. This scheme of enhancing parametric gain, and therefore the generated IDS, in the system by modulating the internal states of a multilevel atomic system has certain obvious advantages over using separate cascading stages in enhancing IDS. The first is the lower optical path loss. The second is a higher squeezing limit with fewer vacuum losses because of a one-stage rubidium cell. The third is that the dressing field can improve the noise figure of the system and make it close to the quantum limit. At the same time, the degree of IDS can be not only greatly enhanced, but also suppressed by simply varying the frequency detunings of the additional driving fields. Compared with the case of a single cell, our model has a lower-pump-power limit and higher-gain saturation limit because of the degenerate multiwave-mixing process. These merits will greatly facilitate the potential applications of such IDS light sources in entanglement imaging [11,12], quantum metrology [16–21], quantum communication [29–32], and quantum information processing [29,32].

II. THEORETICAL MODEL

The five relevant energy levels are $5S_{1/2}$, $F=2(|0\rangle)$; $5S_{1/2}$, $F=3(|1\rangle)$; $5P_{3/2}(|2\rangle)$; $5D_{5/2}(|3\rangle)$; and $5P_{1/2}(|4\rangle)$ in ^{85}Rb, as shown in Fig. 1(b). Levels $|0\rangle \leftrightarrow |2\rangle \leftrightarrow |1\rangle$ form the basic Λ-type three-level system. A strong pump beam $\boldsymbol{E}_1$ (with

*Corresponding author: ypzhang@mail.xjtu.edu.cn

†Corresponding author: mxiao@uark.edu

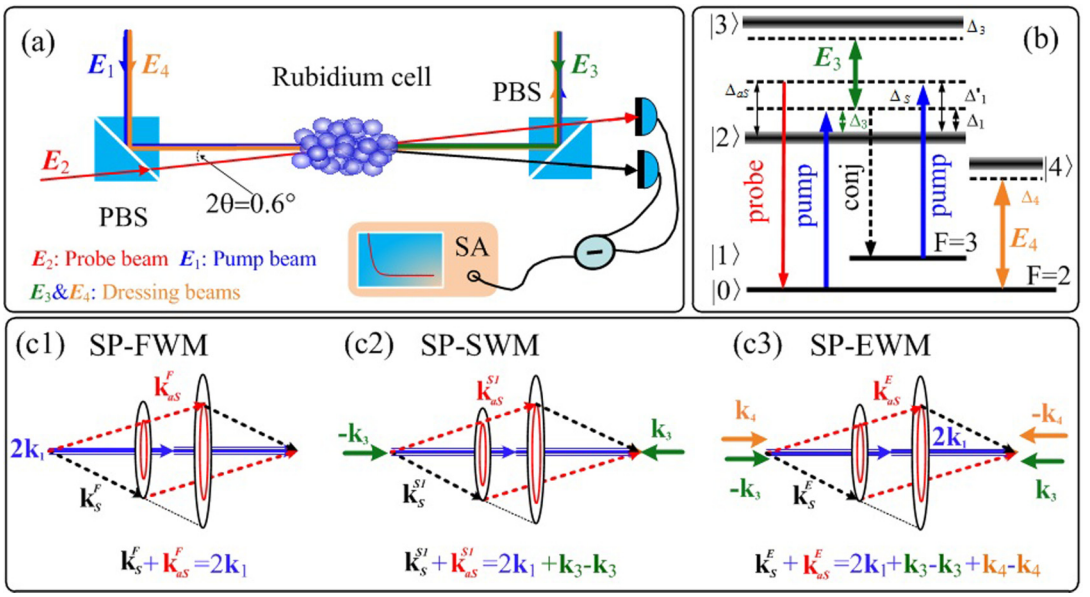

FIG. 1. (a) Experimental setup: PBS, polarizing beam splitter; SA, spectrum analyzer. (b) Energy-level diagram of the (Λ-type ($|0\rangle \leftrightarrow |1\rangle \leftrightarrow |2\rangle$) rubidium atomic system with an $\boldsymbol{E}_3$ ladder-type dressing (between levels $|2\rangle$ and $|3\rangle$) and an $\boldsymbol{E}_4$ V-type dressing (between levels $|0\rangle$ and $|4\rangle$) simultaneously. (c) Phase-matching conditions for the spontaneous parametric (c1) spontaneous FWM, (c2) spontaneous SWM1, and (c) spontaneous EWM processes.

frequency $\omega_1, \mathbf{k}_1$, Rabi frequency G_1, and vertical polarization) is tuned to couple the $D2$ line (780-nm) transition and a weak beam $\boldsymbol{E}_2$ (ω_2, $\mathbf{k}_2$, Rabi frequency G_2, and horizontal polarization) works as a probe field. The detuning $\Delta_i = \Omega_i - \omega_i$ is defined as the difference between the resonant transition frequency Ω_i and the laser frequency ω_i of $\boldsymbol{E}_i$. With the frequency of $\boldsymbol{E}_1$ tuned far away from the resonances, this system forms the standard PA nondegenerate FWM configuration to satisfy the phase-matching condition $\mathbf{k}_S^F + \mathbf{k}_{aS}^F = 2\mathbf{k}_1$ [as shown in Fig. 1(c1)] and produces narrow-band IDS between the parametrically amplified probe (anti-Stokes) and conjugate (Stokes) beams. The generated IDS mainly depends on the gain factor T_F in the anti-Stokes channel. This nonlinear gain factor T_F can be modified by multiple parameters in multilevel coherent atomic systems.

First, one can consider a situation such that there exists n-dressing fields in the system of a three-level Λ-type configuration. The interaction Hamiltonian of the n-dressing PA FWM process can be expressed as (all pump and dressing fields are treated as classical fields)

$$H = i\hbar\kappa^{nd}\hat{a}^\dagger\hat{b}^\dagger + \text{H.c.}, \tag{1}$$

where $\kappa^{nd} = |-i\mu_0\varpi_{S,aS}^2\chi^{nd(3)}E_1{}^2/2k_{S,aS}|$ is the pumping parameter of the n-dressing PA FWM, which depends on the nonlinear susceptibility tensor $\chi^{nd(3)}$ and the pump-field amplitude, with $\varpi_{S,aS}$ the central frequency of the generated Stokes or anti-Stokes signal. In the dressed-state pictures, the third-order nonlinear susceptibility tensor can be expressed as $\chi^{nd(3)} = |N\mu_{20}\mu_{21}\rho_{(S,aS)}^{nd(3)}/\varepsilon_0\hbar E_1^2 G_{S,aS}|$, where $\rho_{(S,aS)}^{nd(3)}$ are the corresponding n-dressing density matrix elements, which can be obtained via perturbation chains $\rho_{11}^{(0)} \xrightarrow{\omega_1} \rho_{21}^{(1)} \xrightarrow{\omega_{aS}} \rho_{01}^{(2)} \xrightarrow{\omega_1} \rho_{21(S)}^{(3)}$ and $\rho_{00}^{(0)} \xrightarrow{\omega_1} \rho_{20}^{(1)} \xrightarrow{\omega_S} \rho_{10}^{(2)} \xrightarrow{\omega_1} \rho_{20(aS)}^{(3)}$. Thus, $\rho_{(S)}^{nd(3)}$ and $\rho_{(aS)}^{nd(3)}$ can be described as

$$\rho_{(S)}^{nd(3)} = -iG_1^2 G_{aS}/d_{21D}d_{01}d_{21}, \tag{2}$$

$$\rho_{(aS)}^{nd(3)} = -iG_1^2 G_S/d_{20D}d_{10D}d_{20}, \tag{3}$$

where $d_{10D} = \Gamma_{10} + i\Delta_1 - i\Delta_s$, $d_{20D} = \Gamma_{20} + i\Delta_1 + G_3^2/\{\Gamma_{30} + i(\Delta_1 + \Delta_3) + G_4^2/[\Gamma_{40} + i(\Delta_1 + \Delta_3 + \Delta_4) + \cdots + G_{n+3}^2/d_{n0}]\}$, $d_{01} = \Gamma_{01} + i\Delta'_{11} - i\Delta_{aS}$, $d_{n1} = \Gamma_{n1} + i(\Delta'_1 + \Delta_3 + \Delta_4 \cdots + \Delta_{n+3})$, $d_{n0} = \Gamma_{n0} + i(\Delta_1 + \Delta_3 + \Delta_4 \cdots + \Delta_{n+3})$, $d_{21} = \Gamma_{21} + i\Delta_1$, and $d_{20} = \Gamma_{20} + i(\Delta_1 - \Delta_S + \Delta_1)$.

The boson-creation (-annihilation) operator satisfies the Heisenberg operator equation of motion in the dipole approximation

$$\frac{d\hat{a}}{dz} = \frac{1}{i\hbar}[\hat{a}, \hat{H}] = \kappa^{nd}\hat{b}^\dagger, \tag{4}$$

$$\frac{d\hat{b}^\dagger}{dz} = \frac{1}{i\hbar}[\hat{b}^\dagger, \hat{H}] = \kappa^{nd}\hat{a}. \tag{5}$$

After some algebra, we can get the anti-Stokes and Stokes fields at the output site of the medium:

$$\hat{a}_{\text{out}} = \cosh(\kappa^{nd}L)\hat{a}_{\text{in}} + \sinh(\kappa^{nd}L)\hat{b}_{\text{in}}^\dagger, \tag{6}$$

$$\hat{b}_{\text{out}}^\dagger = \cosh(\kappa^{nd}L)\hat{b}_{\text{in}}^\dagger + \sinh(\kappa^{nd}L)\hat{a}_{\text{in}}. \tag{7}$$

Moreover, the probe field and vacuum field (i.e., $|\alpha,0\rangle$) are injected into the anti-Stokes and Stokes ports of a spontaneous parametric FWM process, respectively. Then the whole process can be viewed as a PA FWM process. The photon numbers of the output signals at the Stokes and

anti-Stokes ports can be expressed as

$$\langle N_a\rangle = \langle \hat{a}_{\rm out}^{\dagger}\hat{a}_{\rm out}\rangle = \cosh^2(\kappa^{nd}L)\langle \hat{a}_{\rm in}^{\dagger}\hat{a}_{\rm in}\rangle + \sinh^2(\kappa^{nd}L) \approx T_F^{nd}\langle \hat{a}_{\rm in}^{\dagger}\hat{a}_{\rm in}\rangle = T_F^{nd}\alpha^2, \quad (8)$$

$$\langle N_b\rangle = \langle \hat{b}_{\rm out}^{\dagger}\hat{b}_{\rm out}\rangle = \sinh^2(\kappa^{nd}L)\langle \hat{a}_{\rm in}^{\dagger}\hat{a}_{\rm in}\rangle + \cosh^2(\kappa^{nd}L) \approx \left(T_F^{nd}-1\right)\langle \hat{a}_{\rm in}^{\dagger}\hat{a}_{\rm in}\rangle = \left(T_F^{nd}-1\right)\alpha^2. \quad (9)$$

Here we define the n-dressing nonlinear gain coefficient $T_F^{nd} = \cosh^2(\kappa^{nd}L)$. The IDS in n-dressing PA FWM is

$$Sq_F^{nd} = -10\log\left(2T_F^{nd}-1\right). \quad (10)$$

Both the T_F^{nd} and Sq_F^{nd} present in this system increase as the number of dressing beams increases. Similarly, the noise figure of the n-dressed configuration has the form

$$NF^{nd} = \eta\left(2-\frac{2}{T_F^{nd}}+\frac{1}{\eta T_F^{nd}}\right). \quad (11)$$

This means that the dressing field can improve the noise figure under the same η and make it close to the quantum limit.

However, there exist inevitable losses in the system; such losses with vacuum field coupling will make a limit value of the squeezing [24]. If we consider the loss of the system, the vacuum coupling terms (loss terms) $m\hat{c}_1$ and $m\hat{c}_2^{\dagger}$ occur in Eqs. (4) and (5), respectively. The IDS of n-dressing PA FWM can be modified as $Sq_F^{nd} = \log_{10}[(1+m^2)/(2T_F^{nd}-1)]$ in our system. With the increase of separate cascading stages, the loss term in Refs. [22,24] is liable to rapid accumulation, leading to the limit of squeezing. In the cascade system, the squeezing limit depends on the added losses and gain saturation of the system [22]. However, it also mainly depends on the gain saturation in our system with the one-stage rubidium cell, which means we have a higher-limit value.

We conjecture that there is a relation between n-dressing PA FWM and the high-order wave-mixing nonlinear process. One may find that n-dressed PA FWM can be converted into a superposition of a series of special multiwave mixing (MWM) under approximate conditions [33,34]. Correspondingly, $\rho_{(S,aS)}^{nd(3)}$ can be broken down into a superposition of FWM and special $(n-1)$-dressing six-wave mixing (SWM):

$$\rho_{(S)}^{nd(3)} = \rho_{(S)}^{\prime(3)} + \left(-G_3^2/d_{21}d_{31}\right)\rho_{(S)}^{\prime(3)} = \rho_{(S)}^{\prime(3)} + \rho_{(S)}^{(n-1)d(5)}, \quad (12)$$

$$\rho_{(aS)}^{nd(3)} = \rho_{(aS)}^{\prime(3)} + \left(-G_3^2/d_{20}d_{30}\right)\rho_{(aS)}^{\prime(3)} = \rho_{(aS)}^{\prime(3)} + \rho_{(aS)}^{(n-1)d(5)}, \quad (13)$$

where $d_{31} = G_4^2/[\Gamma_{41} + i(\Delta_1' + \Delta_3 + \Delta_4)\cdots + G_{n+3}^2/d_{n1}]$, $d_{21} = \Gamma_{31} + i(\Delta_1' + \Delta_3)$, $d_{20} = \Gamma_{30} + i(\Delta_1 + \Delta_3)$, and $d_{30} = G_4^2/[\Gamma_{40} + i(\Delta_1 + \Delta_3 + \Delta_4)\cdots + G_{n+3}^2/d_{n0}]$.

For the ladder-type dressing, $\boldsymbol{E}_3$ couples the transition $|2\rangle \leftrightarrow |3\rangle$ and creates the dressed states $|G3_{\pm}\rangle$. If we set $|2\rangle$ as the frequency reference point, the Hamiltonian can be written as

$$H = \hbar\begin{bmatrix} 0 & G_3 \\ G_3^* & -\Delta_3 \end{bmatrix}, \quad (14)$$

from the equation $H|G3_{\pm}\rangle = \lambda_{\pm}|G3_{\pm}\rangle$, and we can obtain $\lambda_{\pm} = [-\Delta_3 \pm \sqrt{\Delta_3^2 + 4|G_3|^2}]/2$. According to the dressed-state picture, the enhancement and suppression conditions are $\Delta_1+\Delta_3 \pm \sqrt{\Delta_3^2+4|G_3|^2}/2 = 0$ and $\Delta_1+\Delta_3 = 0$, respectively. Here the n-dressing nonlinear gain coefficient is related to the matrix element $\rho_{(S,aS)}^{nd(3)}$ as $T_F^{nd} = \cosh^2(\kappa^{nd}L)$, where $\kappa^{nd} \propto |\rho_{(S,aS)}^{\prime(3)} + \rho_{(S,aS)}^{(n-1)d(5)}|$. When the dressed field $\boldsymbol{E}_3$ detuning meets the enhancement condition, one can obtain the maximum nonlinear gain coefficient $T_F^{nd} = \cosh^2(\kappa_m L)$, where $\kappa_m \propto |\rho_{(S,aS)}^{\prime(3)}| + |\rho_{(S,aS)}^{(n-1)d(5)}|$ [constructive interference between FWM and $(n-1)$-dressing SWM]. The IDS in n-dressing FWM can be divided into two parts: FWM and $(n-1)$-dressing SWM. The relationship can be written as $Sq_F^{nd} = Sq_F + Sq_S^{(n-1)d} - \log_{10}2$ and $Sq_F^{nd} = Sq_F - Sq_S^{(n-1)d} + \log_{10}2$, which correspond to dressed enhancement and suppression conditions, respectively.

If we successively extend this limit to all dressing field, Eqs. (2) and (3) can be rewritten as

$$\rho_{(S)}^{nd(3)} = \rho_{(S)}^{\prime(3)} + \rho_{(S)}^{\prime(5)} + \cdots + \rho_{(S)}^{\prime(2n+3)}, \quad (15)$$

$$\rho_{(aS)}^{nd(3)} = \rho_{(aS)}^{\prime(3)} + \rho_{(aS)}^{\prime(5)} + \cdots + \rho_{(aS)}^{\prime(2n+3)}. \quad (16)$$

The n-dressing FWM process corresponds to the sum of $n+1$ nonlinear processes, i.e., FWM + SWM + EWM + $\cdots$ $+(2n+4)$ wave mixing (where EWM denotes eight-wave mixing). Here $\rho_{(S)}^{\prime(2n+3)}$ and $\rho_{(aS)}^{\prime(2n+3)}$ are the $(2n+4)$-wave mixing signal processes, which can be deduced via the perturbation chains $\rho_{11}^{(0)} \xrightarrow{\omega_1} \rho_{21}^{(1)} \xrightarrow{\omega_3} \rho_{31}^{(2)} \cdots \xrightarrow{-\omega_3} \rho_{21}^{(2n+1)} \xrightarrow{(\omega_{aS})*} \rho_{01}^{(2n+2)} \xrightarrow{\omega_1} \rho_{21(S)}^{\prime(2n+3)}$ and $\rho_{00}^{(0)} \xrightarrow{\omega_1} \rho_{20}^{(1)} \xrightarrow{\omega_3} \rho_{30}^{(2)} \cdots \xrightarrow{-\omega_3} \rho_{20}^{(2n+1)} \xrightarrow{(\omega_s)*} \rho_{10}^{(2n+2)} \xrightarrow{\omega_1} \rho_{20(aS)}^{\prime(2n+3)}$, respectively, where $\rho_{(s)}^{\prime(2n+3)} = (-1)^n[(G_3^2/d_{21}d_{31})(G_4'^2/d_{31}d_{41})\cdots(G_{n+3}^2/d_{(n+2)1}d_{(n+3)1})]\rho_{(s)}^{\prime(3)}$ and $\rho_{(aS)}^{\prime(2n+3)} = (-1)^n[(G_3^2/d_{20}d_{30})(G_4'^2/d_{30}d_{40})\cdots(G_{n+3}^2/d_{(n+2)0}d_{(n+3)0})]\rho_{(aS)}^{\prime(3)}$.

The interaction Hamiltonian (1) of the n-dressing PA FWM process can be rewritten as

$$H = i\hbar\kappa_3'\hat{a}^{\dagger}\hat{b}^{\dagger} + \cdots + i\hbar\kappa_{2n+3}'\hat{a}^{\dagger}\hat{b}^{\dagger} + \text{H.c.} \quad (17)$$

Accordingly, the boson-creation and -annihilation operators that satisfy the Heisenberg operator equation of motion in the dipole approximation become, respectively,

$$\frac{d\hat{a}}{dz} = \frac{1}{i\hbar}[\hat{a},\hat{H}] = (\kappa_3' + \kappa_5' + \cdots + \kappa_{2n+3}')\hat{b}^{\dagger}, \quad (18)$$

$$\frac{d\hat{b}^{\dagger}}{dz} = \frac{1}{i\hbar}[\hat{b}^{\dagger},\hat{H}] = (\kappa_3' + \kappa_5' + \cdots + \kappa_{2n+3}')\hat{a}. \quad (19)$$

After similar mathematical operations with Eqs. (8) and (9), the IDS relationships between n-dressing FWM and coexisting $n+1$ MWMs can be written as

$$Sq_F^{nd} = Sq_F + Sq_S + Sq_E^{(n-2)d} - 2\log_{10}2 = \cdots = Sq_F + \cdots + Sq_{(2n+4)} - n\log_{10}2, \quad (20)$$

$$Sq_F^{nd} = Sq_F - Sq_S - Sq_E^{(n-2)d} + 2\log_{10}2 = \cdots = Sq_F - \cdots - Sq_{(2n+4)} + n\log_{10}2, \quad (21)$$

which correspond to dressed enhancement (constructive interference) and suppression conditions (destructive interference), respectively.

Next, let us turn our attention to energy-level modulation (one-beam dressing) with an additional laser beam $\boldsymbol{E}_4$ (ω_4, $\mathbf{k}_4$, G_4, and Δ_4) in the V-type dressing scheme [Fig. 1(b)]. It behooves us to think of the population transfer effect when the dressed field $\boldsymbol{E}_4$ acts on the ground state. We assume that T^p results from the initial population probability in each energy level expressed as

$$T^p \propto \rho_{22}^{(2)} + \rho_{44}^{(2)} + \rho_{22}^{(4)} + \rho_{44}^{(4)}, \tag{22}$$

where $\rho_{22}^{(2)} = -G_1^2/d_{20}\Gamma_{22}$, $\rho_{44}^{(2)} = -G_4^2/d_{40}\Gamma_{44}$, $\rho_{22}^{(4)} = G_1^2G_4^2/d_{40}\Gamma_{00}d_{20}\Gamma_{22}$, $d_{40} = \Gamma_{40} + i\Delta_4$, and $\rho_{44}^{(4)} = G_1^2G_4^2/d_{20}\Gamma_{00}d_{40}\Gamma_{44}$ (deduced via perturbation chains $\rho_{00}^{(0)} \xrightarrow{\omega_1} \rho_{20}^{(1)} \xrightarrow{(\omega_1)*} \rho_{22}^{(2)}$, $\rho_{00}^{(0)} \xrightarrow{\omega_4} \rho_{40}^{(1)} \xrightarrow{(\omega_4)*} \rho_{44}^{(2)}$, $\rho_{00}^{(0)} \xrightarrow{\omega_4} \rho_{40}^{(1)} \xrightarrow{(\omega_4)*} \rho_{00}^{(2)} \xrightarrow{\omega_1} \rho_{20}^{(3)} \xrightarrow{(\omega_1)*} \rho_{22}^{(4)}$, and $\rho_{00}^{(0)} \xrightarrow{\omega_1} \rho_{20}^{(1)} \xrightarrow{(\omega_1)*} \rho_{00}^{(2)} \xrightarrow{\omega_4} \rho_{40}^{(3)} \xrightarrow{(\omega_4)*} \rho_{44}^{(4)}$, respectively). So the $\boldsymbol{E}_4$-dressed nonlinear gain T_{F2}^{1d} will be modified by the population gain T^p and the total nonlinear gain becomes $T_{F'}^{1d} = T^p + T_{F2}^{1d}$. Therefore, we modify the squeezing formula under the condition of dressed enhancement and suppression as $Sq_{F'}^{1d} = Sq_{F'} + Sq_{S2} - \log_{10} 2$ and $Sq_{F'}^{1d} = Sq_{F'} - Sq_{S2} + \log_{10} 2$, respectively.

Note that we have used different orders of MWM processes to describe the modified (dressed) PA FWM processes, which give a clear physical picture for the complicated situations and is valid under certain approximations of the dressing fields [33,34]. With the clear decompositions of the dressed-state formulism for the multibeam-dressed PA FWM, we can better identify the contributions of the modified IDS from different wave-mixing processes. Such methods show a robust and efficient way to produce a high degree of IDS.

III. EXPERIMENT RESULTS

As mentioned above, there are two ways to dress the Λ-type three-level ($|0\rangle \leftrightarrow |1\rangle \leftrightarrow |2\rangle$) system, one by applying $\boldsymbol{E}_3$ between levels $|2\rangle$ and $|1\rangle$ (i.e., ladder-dressing configuration) and another by applying $\boldsymbol{E}_4$ between levels $|0\rangle$ and $|4\rangle$ (V-dressing configuration), as shown in Fig. 1(b), which modify the original PA FWM process differently and therefore provide different enhancement factors for IDS. In the following, we consider their effects separately. We use light of 500 mW from a cw Ti:sapphire laser as the 780-nm pump beam ($\boldsymbol{E}_1$) and another light up to 0.2 mW from an external cavity diode laser as the 780-nm probe beam ($\boldsymbol{E}_2$). They couple with the Λ-type atomic system in a naturally abundant rubidium vapor cell by a polarizing beam splitter. The vapor cell is wrapped with μ-metal sheets to shield the stray magnetic field from the environment and heated to 125 °C to provide an atomic density of 3×10^{13} cm^{-3}. The beam $\boldsymbol{E}_2$ propagates in the same direction as $\boldsymbol{E}_1$ with a small angle of 0.26°. These two laser beams form the standard double-Λ configuration and produce the PA FWM IDS. When $\boldsymbol{E}_4$ (795 nm, 4 mW) is added to $\boldsymbol{E}_1$ (in the same direction) and $\boldsymbol{E}_3$ (776 nm, 8 mW) counterpropagates with $\boldsymbol{E}_1$, they establish two electromagnetically induced transparency windows in the system and significantly modify (dressing) the original PA FWM process [28,35]. The dressing fields of 776 and 795 nm are provided by two Toptica lasers. Their frequencies are locked but phases are unlocked. The spatial alignments of the beams are shown in Fig. 1(a). The output probe and conjugate beams are detected by two balanced photodetectors. The difference of the two detected signals is sent to a radio-frequency spectrum analyzer with a resolution bandwidth of 300 kHz and a video bandwidth of 10 kHz. All intensity difference measurements presented in this paper are taken at an analysis frequency of 1 MHz.

Figure 2 shows PA FWM signals in the probe and corresponding conjugate channels in the three-level Λ-type ^{85}Rb atomic system, respectively, with and without the $\boldsymbol{E}_3$ beam. With $\boldsymbol{E}_3$ off and the pump field detuning Δ_1 detuned to ~1.12 GHz, we scan the probe field $\boldsymbol{E}_2$ over 8 GHz across the $D2$ line and observe a number of features in transmission and its conjugate channels, as shown in Figs. 2(a1) and 2(a3), respectively. When $\boldsymbol{E}_3$ turns on, as shown in Fig. (c2), the one-beam dressing FWM [coexisting FWM and SWM1, with phase-matching condition $\mathbf{k}_S^{S1} + \mathbf{k}_{aS}^{S1} = 2\mathbf{k}_1 + \mathbf{k}_3 - \mathbf{k}_3$, Fig. 1(c2)] [28] signal in Fig. 2(a2) gets stronger than that in Fig. 2(a1), which indicates an enhanced FWM process. The $\boldsymbol{E}_3$-dressed PA FWM signal is enhanced due to the constructive interference

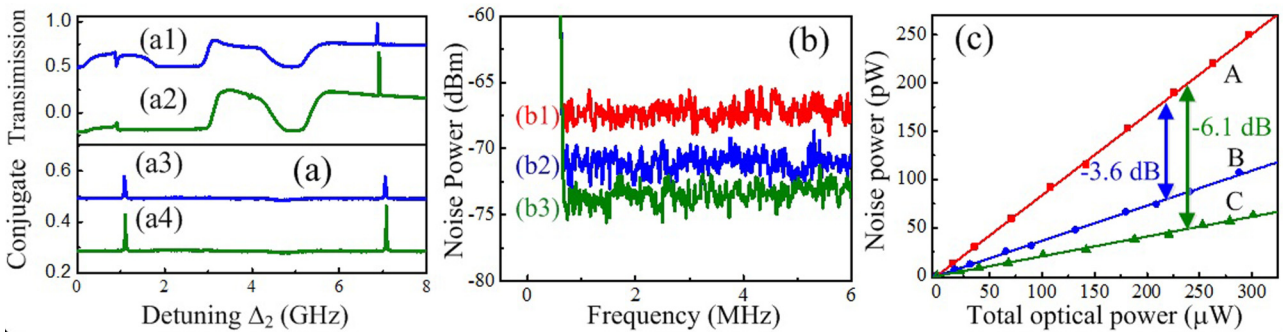

FIG. 2. (a) Measured probe transmission ($\boldsymbol{E}_{aS}$) and corresponding conjugate ($\boldsymbol{E}_S$) signal versus probe frequency detuning with (a1) and (a3) $\boldsymbol{E}_3$ off and (a2) and (a4) $\boldsymbol{E}_3$ on, for $\Delta_1 = 1.12$ GHz and $\Delta_3 = -1$ GHz. (b) Relative intensity noise levels versus spectrum analyzer frequency for (b1) SQL, (b2) FWM, and (b3) dressed FWM (FWM plus SWM1) when $\boldsymbol{E}_3$ is applied, and electronic noise. (c) Relative intensity noise power at different total optical power for curve A, SNL (diamonds); curve B, FWM (circles); and curve C, single-dressing FWM (triangles). All three of these noise power curves fit to straight lines. The electronic noise floor and background noise are subtracted from all of the traces and data points.

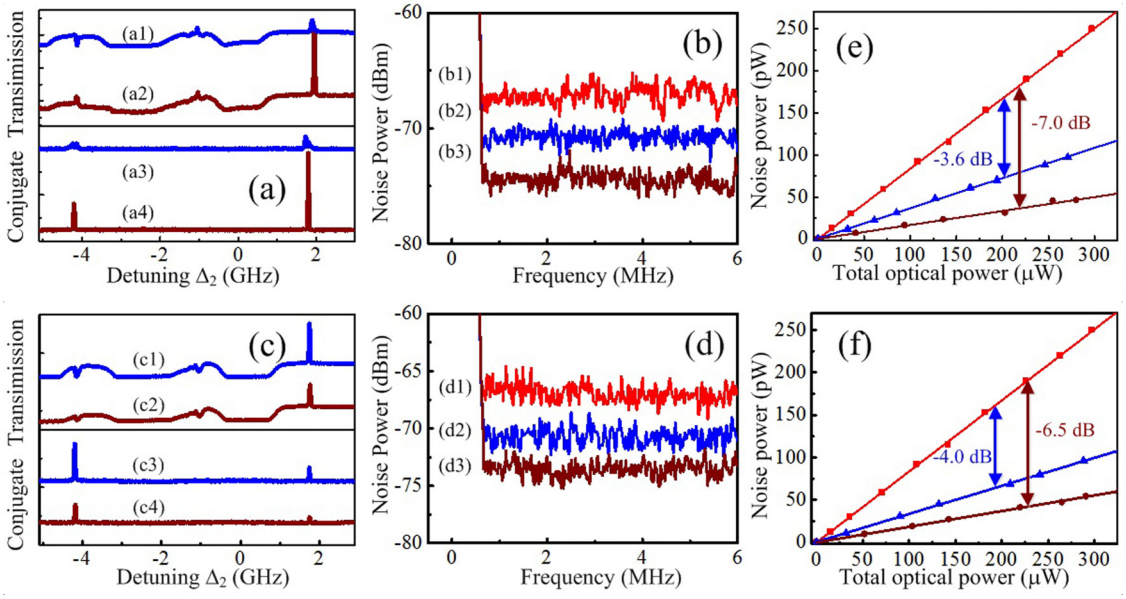

FIG. 3. Same as Fig. 2 but with (a1) and (a3) $\boldsymbol{E}_4$ off and (a2) and (a4) $\boldsymbol{E}_4$ on, for $\Delta_1 = 1.12$ GHz and $\Delta_4 = -1$ GHz. (b) Relative intensity noise levels versus spectrum analyzer frequency for (b1) SQL, (b2) FWM, and (b3) dressed FWM (FWM plus SWM2) when field $\boldsymbol{E}_4$ is applied. (c) and (d) Same as (a) and (b) but for (c) $\Delta_1 = 1.15$ GHz and (d) $\Delta_4 = 1.15$ GHz, respectively. (e) Relative intensity noise power at different total optical power for SNL (diamonds), FWM (triangles), and enhanced $\boldsymbol{E}_4$-dressing FWM (circles). (f) Same as (e) except that it is suppressed $\boldsymbol{E}_4$-dressing FWM. All these noise power curves fit to straight lines. The electronic noise floor and background noise are subtracted from all of the traces and data points.

between FWM and SWM1, satisfying the dressed enhancement condition $\Delta_1+\Delta_3 \pm \sqrt{\Delta_3^2+4|G_3|^2}/2 = 0$. Similar to the probe channel, the corresponding conjugate signal is also enhanced due to the existing PA SWM1 process, as shown in Fig. 2(a4). So the dressed gain coefficient is enhanced compared to the gain coefficient without the $\boldsymbol{E}_3$ beam [Fig. 2(a3)].

Subsequently, the noise spectra of the relative intensities between the probe and conjugate channels are measured. First, $\boldsymbol{E}_1$ passes through an acousto-optic modulator of 1.5 GHz twice to have a frequency difference of 3 GHz. The beam is then injected into the probe channel and the field $\boldsymbol{E}_2$ is off. To calibrate the standard quantum limit (SQL) for the total optical power arriving at the photodetectors, a coherent beam with the same power is split by a 50/50 beam splitter, directing the resulting beams into a balanced and amplified photodetector with a transimpedance gain of 10^5 V/A and 81% quantum efficiency. The measured IDS of the PA FWM signal [Fig. 2(b2)] is (-3.6 ± 0.4) dB below the normalized SQL. With the dressing field $\boldsymbol{E}_3$ on, the measured IDS of the $\boldsymbol{E}_3$-dressed FWM signal [Fig. 2(b3)] is about (-6.1 ± 0.4) dB below the SQL, which indicates that the degree of IDS is significantly increased by the enhanced nonlinear gain coefficient due to the $\boldsymbol{E}_3$ dressing effect, as shown in Fig. 2(b3). Furthermore, one can infer IDS of the pure PA SWM1 to be (-2.8 ± 0.4) dB.

To better show the squeezing enhancement as predicted by the theory, we measure the relative intensity noise power for the FWM [curve B in Fig. 2(c)] and single-dressing FWM (curve C) at 1 MHz as a function of the total optical power impinging on the photodetectors. We also record the noise powers of a coherent beam at different optical powers using the shot-noise limit (SNL) measurement method described above (curve A). We can see that the ratios of the slopes for curves B and A and curves C and A are 0.437 ± 0.038 and 0.245 ± 0.038, respectively, which indicate the degrees of squeezing of the FWM and single-dressed FWM to be about (-3.6 ± 0.4) dB and (-6.1 ± 0.4) dB, respectively. The optical path transmission is 80%, resulting in a total detection efficiency of 64.8%; the uncertainty is estimated at 1 standard deviation. The inferred degrees of squeezing for the FWM and $\boldsymbol{E}_3$-dressed FWM beams are -8.5 and -11.0 dB after correction for losses, respectively.

Next we consider the case with $\boldsymbol{E}_4$-dressed PA FWM instead of $\boldsymbol{E}_3$. Figures 3(a2) and 3(c2) show that, compared to the original PA FWM [Figs. 3(a1) and 3(c1)], the $\boldsymbol{E}_4$-dressed FWM signal in the probe channel can be either enhanced or suppressed. The field $\boldsymbol{E}_4$ dresses the ground state $|0\rangle$ and creates the dressed states $|G_{4\pm}\rangle$. Thus, due to the fulfillments of dressed enhancement and suppression conditions, i.e., $\Delta_1 - \Delta_4 \pm \sqrt{\Delta_4^2+4|G_4|^2}/2 = 0$ and $\Delta_1 + \Delta_4 = 0$, the PA FWM signal can be either enhanced or suppressed [27,28]. The increase or decrease of the probe and conjugate field intensities [Figs. 3(a2) and 3(c2)] is caused by constructive or destructive interference between the generated FWM and SWM2 fields. Therefore, the corresponding dressed gain T_{F2}^{1d} becomes large or small accordingly.

Figures 3(b) and 3(d) depict the measured IDS of $\boldsymbol{E}_4$-dressed FWM, corresponding to enhanced [Fig. 3(b)] and suppressed [Fig. 3(d)] conditions, respectively. The measured degree of IDS for this $\boldsymbol{E}_4$-dressed FWM [Fig. 3(b3)] is (-7.0 ± 0.4) dB, which is much larger than that of the original PA FWM [(-3.6 ± 0.4) dB] [Fig. 3(b2)]. The relative intensity

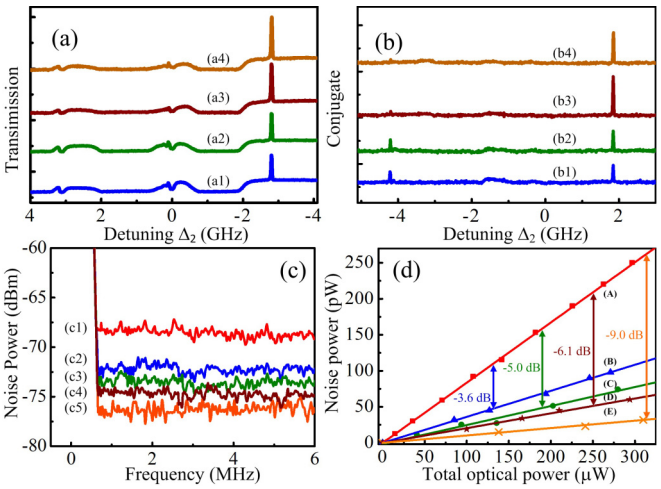

FIG. 4. (a) Measured probe transmission signal $\boldsymbol{E}_{aS}$ versus the probe detuning with (a1) $\boldsymbol{E}_3$ and $\boldsymbol{E}_4$ off, (a2) $\boldsymbol{E}_3$ on, (a3)$\boldsymbol{E}_4$ on, and (a4) $\boldsymbol{E}_3$ and $\boldsymbol{E}_4$ both on, for $\Delta_1 = 1.12$ GHz, $\Delta_3 = -0.9$ GHz, and $\Delta_4 = 0.95$ GHz. (b1)–(b4) Corresponding conjugate signal $\boldsymbol{E}_S$ of (a1)–(a4), respectively. (c) Relative intensity noise levels versus spectrum analyzer frequency for (c1) SQL, (c2) FWM, (c3) $\boldsymbol{E}_3$-dressed FWM, (c4) $\boldsymbol{E}_4$-dressed FWM, and (c5) $\boldsymbol{E}_3$- and $\boldsymbol{E}_4$-dressed FWM (FWM plus SWM plus EWM). (d) Relative intensity noise power at different total optical power for curve A, SNL (diamonds); curve B, FWM (triangles); curve C, $\boldsymbol{E}_3$-dressing FWM (circles); curve D, $\boldsymbol{E}_4$-dressing FWM (pentagons); and curve E, double-dressing FWM (crosses). All five of these noise power curves fit to straight lines. The electronic noise floor and background noise are subtracted from all of the traces and data points.

noise powers for FWM (triangles) and $\boldsymbol{E}_4$-dressed FWM (circular) are shown in Fig. 3(e) with the change in total optical power. Since they are similar to Fig. 2(c), we will not repeat here. Moreover, the inferred -3.7 dB IDS for the PA SWM2 process is larger than the -2.8 dB IDS for the PA SWM1 process with $\boldsymbol{E}_3$ dressing shown in Fig. 2(b3). The reason is that $\boldsymbol{E}_4$ has the effects of both population transfer and dressing [Eq. (22)] while $\boldsymbol{E}_3$ only has the dressing gain, resulting in a much larger total nonlinear gain $T_{F'}^{1d}$ for the $\boldsymbol{E}_4$-dressed case.

However, due to the existing population gain T^p for the V-type dressing scheme, the $\boldsymbol{E}_4$-dressed PA FWM cannot realize a suppression of IDS below the original PA FWM value. In fact, under the suppressed gain condition (destructive interference between the FWM and SWM2 fields), the measured IDS of the $\boldsymbol{E}_4$-dressed PA FWM is still as large as (-6.5 ± 0.4) dB [Fig. 3(d3)]. Figure 3(f) shows the corresponding dependences of SNL, FWM, and $\boldsymbol{E}_4$-dressed FWM signals on optical power.

Finally, let us consider the case with both $\boldsymbol{E}_3$ and $\boldsymbol{E}_4$ dressing fields on at the same time for the five-level system, as shown in Fig. 1(b), with phase-matching conditions given in Fig. 1(c3). Figures 4(a) and 4(b) show modified PA FWM signals in the probe and conjugate channels, respectively, when a different beam or beams are blocked. With the frequency detunings of $\boldsymbol{E}_3$ and $\boldsymbol{E}_4$ set to be -0.9 and 0.95 GHz, the intensity of dressed PA FWM is expected to increase relative to Fig. 4(a1), as shown in Figs. 4(a2) and 4(a3), respectively. Similar to Figs. 2(a2) and 3(a2), two newly generated PA SWM signals, i.e., SWM1 and SWM2, increase in Figs. 4(a2) and 4(a3). In particular, with $\boldsymbol{E}_3$ and $\boldsymbol{E}_4$ both on simultaneously, a two-beam-dressed FWM signal in Fig. 4(a4) is greatly enhanced, which is the mixture of one pure PA FWM, two SWMs, and one EWM (with phase-matching condition $\mathbf{k}_S^E + \mathbf{k}_{aS}^E = 2\mathbf{k}_1 + \mathbf{k}_3 - \mathbf{k}_3 + \mathbf{k}_4 - \mathbf{k}_4$) processes. At the same time, the intensity of the two-beam-dressed conjugate signal ($\boldsymbol{E}_S$) is also changed accordingly, as shown in Fig. 4(b). So the two-beam dressing gain T_F^{2d} is significantly enhanced.

Figure 4(c) presents the measured degrees of IDS for modified PA FWM signals in Figs. 4(a) and 4(b). First, with all external dressing fields ($\boldsymbol{E}_3$ and $\boldsymbol{E}_4$) blocked, the IDS of pure PA FWM is measured to be (-3.6 ± 0.4) dB [Fig. 4(c2)]. The curve (c1) gives the SQL. When either $\boldsymbol{E}_3$ or $\boldsymbol{E}_4$ is on, the measured IDS of one-beam-dressed FWM is (5.0 ± 0.4) dB [Fig. 4(c3)] or (6.1 ± 0.4) dB [Fig. 4(c4)], respectively. When both dressing fields ($\boldsymbol{E}_3$ and $\boldsymbol{E}_4$) are on at the same time, the measured IDS of two-beam-dressed FWM [Fig. 4(c5)] reaches (-8.1 ± 0.4) dB. Their corresponding dependences of the SNL, FWM, $\boldsymbol{E}_3$-dressed FWM, $\boldsymbol{E}_4$-dressed FWM, and double-dressed FWM signals on optical power are shown in Fig. 4(d). After fitting all five of these noise power curves to straight lines, we find that the ratios of slopes between curves B, C, D, E, and A are equal to 0.436 ± 0.038, 0.316 ± 0.038, 0.245 ± 0.038, and 0.126 ± 0.038, respectively, which shows that the degrees of IDS of the twin beams are about (-3.6 ± 0.4) dB, (-5.0 ± 0.4) dB, (-6.1 ± 0.4) dB, and (-9.0 ± 0.4) dB, respectively. This largely increased degree of IDS is caused by the enhancement in two-beam-dressed PA FWM gain with coexisting and constructive interference PA FWM, SWM, and EWM processes in the system. The inferred degree of IDS for the pure PA EWM is (-2.3 ± 0.4) dB. Moreover, the total degree of IDS can be easily controlled and modulated by adjusting the frequency detunings of the dressing fields.

IV. CONCLUSION

We have observed the enhanced IDS for single- and double-beam-modulated PA FWM processes in the same hot atomic system. Compared to the simple PA FWM case (with -3.6 dB IDS), the degrees of IDS for $\boldsymbol{E}_3$- are $\boldsymbol{E}_4$-modulated PA FWM processes are measured to be -6.1 and -7.0 dB, respectively. The degree of IDS for the two-beam-dressed PA FWM process gets up to -9.0 dB, which indicates that the generated higher-order PA MWM processes contribute to the total parametric gain and therefore the quantum noise suppression (or enhanced IDS). Under different dressing frequency detunings, the generated high-order nonlinear signals can interfere either constructively, which enhances the total parametric gain, or destructively, which reduces the total gain. Our current experiment demonstrates a robust and efficient way to produce high degree of IDS on an integrated platform, which can find potential applications in quantum metrology and gravitational wave detection [20].

ACKNOWLEDGMENTS

This work was supported by the National Key R&D Program of China (Grant No. 2017YFA0303700), the National Nature Science Foundation of China (Grants No. 61605154 and No. 11474228), the Key Science and Technological

Innovation Team of Shannxi Province (Grant No. 2014KCT-10), the Natural Science Foundation of ShaanXi Province (Grants No. 2017JQ6039 and No. 2017JZ019), and China Postdoctoral Science Foundation (Grants No. 2016M600776, No. 2016M600777, No. 2017T100734).

D.Z. and C.L. contributed equally to this work.

[1] A. Heidmann, R. J. Horowicz, S. Reynaud, E. Giacobino, C. Fabre, and G. Camy, Phys. Rev. Lett. **59**, 2555 (1987).
[2] P. H. Ribeiro, C. Schwob, A. Maître, and C. Fabre, Opt. Lett. **22**, 1893 (1997).
[3] K. S. Zhang, T. Coudreau, M. Martinelli, A. Maître, and C. Fabre, Phys. Rev. A **64**, 033815 (2001).
[4] P. G. Kwiat, K. Mattle, H. Weinfurter, A. Zeilinger, A. V. Sergienko, and Y. H. Shih, Phys. Rev. Lett. **75**, 4337 (1995).
[5] H. Hübel, D. R. Hamel, A. Fedrizzi, S. Ramelow, K. J. Resch, and T. Jennewein, Nature (London) **466**, 601 (2010).
[6] L. K. Shalm, D. R. Hamel, Z. Yan, C. Simon, K. J. Resch, and T. Jennewein, Nat. Phys. **9**, 19 (2013).
[7] G. B. Lemos, V. Borish, G. D. Cole, S. Ramelow, R. Lapkiewicz, and A. Zeilinger, Nature (London) **512**, 409 (2014).
[8] C. F. McCormick, V. Boyer, E. Arimondo, and P. D. Lett, Opt. Lett. **32**, 178 (2007).
[9] C. F. McCormick, A. M. Marino, V. Boyer, and P. D. Lett, Phys. Rev. A **78**, 043816 (2008).
[10] Q. Glorieux, L. Guidoni, S. Guibal, J. Likforman, and T. Coudreau, Phys. Rev. A **84**, 053826 (2011).
[11] V. Boyer, A. M. Marino, R. C. Pooser, and P. D. Lett, Science **321**, 544 (2008).
[12] M. W. Holtfrerich, M. Dowran, R. Davidson, B. J. Lawrie, R. C. Pooser, and A. M. Marino, Optica **3**, 985 (2016).
[13] R. M. Camacho, P. K. Vudyasetu, and J. C. Howell, Nat. Photon. **3**, 103 (2009).
[14] A. M. Marino, R. C. Pooser, V. Boyer, and P. D. Lett, Nature (London) **457**, 859 (2009).
[15] J. B. Clark, R. T. Glasser, Q. Glorieux, and P. D. Lett, Nat. Photon. **8**, 515 (2014).
[16] V. Giovannetti, S. Lloyd, and L. Maccone, Phys. Rev. Lett. **96**, 010401 (2006).
[17] R. C. Pooser and B. Lawrie, ACS Photon. **3**, 8 (2016).
[18] R. C. Pooser and B. Lawrie, Optica **2**, 393 (2015).
[19] M. Napolitano, M. Koschorreck, B. Dubost, N. Behbood, R. J. Sewell, and M. W. Mitchell, Nature (London) **471**, 486 (2011).
[20] F. Hudelist, J. Kong, C. Liu, J. Jing, Z. Y. Ou, and W. Zhang, Nat. Commun. **5**, 3049 (2014).
[21] H. Wang, A. M. Marino, and J. Jing, Appl. Phys. Lett. **107**, 121106 (2015).
[22] Z. Qin, L. Cao, H. Wang, A. M. Marino, W. Zhang, and J. Jing, Phys. Rev. Lett. **113**, 023602 (2014).
[23] X. Jia, Z. Yan, Z. Duan, X. Su, H. Wang, C. Xie, and K. Peng, Phys. Rev. Lett. **109**, 253604 (2012).
[24] D. Wang, Y. Zhang, and M. Xiao, Phys. Rev. A **87**, 023834 (2013).
[25] M. Fleischhauer, A. Imamoglu, and J. P. Marangos, Rev. Mod. Phys. **77**, 633 (2005).
[26] Y. Zhang, A. W. Brown, and M. Xiao, Phys. Rev. Lett. **99**, 123603 (2007).
[27] Y. Zhang, U. Khadka, B. Anderson, and M. Xiao, Phys. Rev. Lett. **102**, 013601 (2009).
[28] H. Kang, G. Hernandez, and Y. Zhu, Phys. Rev. Lett. **93**, 073601 (2004).
[29] A. I. Lvovsky and M. G. Raymer, Rev. Mod. Phys. **81**, 299 (2009).
[30] A. Einstein, B. Podolsky, and N. Rosen, Phys. Rev. **47**, 777 (1935).
[31] L. Davidovich, Rev. Mod. Phys. **68**, 127 (1996).
[32] C. Weedbrook, S. Pirandola, R. García-Patrón, N. J. Cerf, T. C. Ralph, J. H. Shapiro, and S. Lloyd, Rev. Mod. Phys. **84**, 621 (2012).
[33] Y. Zhang and M. Xiao, Opt. Express **15**, 7182 (2007).
[34] Z. Zuo, J. Sun, X. Liu, Q. Jiang, G. Fu, L. A. Wu, and P. Fu, Phys. Rev. Lett. **97**, 193904 (2006).
[35] Y. Wu, J. Saldana, and Y. Zhu, Phys. Rev. A **67**, 013811 (2003).